JBC RESEARCH ARTICLE

Noncovalent interactions that tune the reactivities of the flavins in bifurcating electron transferring flavoprotein

Received for publication, March 13, 2023, and in revised form, April 20, 2023 Published, Papers in Press, April 27, 2023,
https://doi.org/10.1016/j.jbc.2023.104762

María González-Viegas[1,2], **Rajiv K. Kar**[1], **Anne-Frances Miller**[1,3,*], **and Maria-Andrea Mroginski**[1,*]

From the [1]*Department of Chemistry, Technische Universität - Berlin, Berlin, Germany;* [2]*Department of Physics, Freie Universität Berlin, Berlin, Germany;* [3]*Department of Chemistry, University of Kentucky, Lexington Kentucky, USA*

Reviewed by members of the JBC Editorial Board. Edited by Joan B. Broderick

Bifurcating electron transferring flavoproteins (Bf-ETFs) tune chemically identical flavins to two contrasting roles. To understand how, we used hybrid quantum mechanical molecular mechanical calculations to characterize noncovalent interactions applied to each flavin by the protein. Our computations replicated the differences between the reactivities of the flavins: the electron transferring flavin (^{ET}flavin) was calculated to stabilize anionic semiquinone (ASQ) as needed to execute its single-electron transfers, whereas the Bf flavin (^{Bf}flavin) was found to disfavor the ASQ state more than does free flavin and to be less susceptible to reduction. The stability of ^{ET}flavin ASQ was attributed in part to H-bond donation to the flavin O2 from a nearby His side chain, *via* comparison of models employing different tautomers of His. This H-bond between O2 and the ET site was uniquely strong in the ASQ state, whereas reduction of ^{ET}flavin to the anionic hydroquinone (AHQ) was associated with side chain reorientation, backbone displacement, and reorganization of its H-bond network including a Tyr from the other domain and subunit of the ETF. The Bf site was less responsive overall, but formation of the ^{Bf}flavin AHQ allowed a nearby Arg side chain to adopt an alternative rotamer that can H-bond to the ^{Bf}flavin O4. This would stabilize the anionic ^{Bf}flavin and rationalize effects of mutation at this position. Thus, our computations provide insights on states and conformations that have not been possible to characterize experimentally, offering explanations for observed residue conservation and raising possibilities that can now be tested.

Electron transferring flavoproteins (ETFs) have been known since the 1950s to shuttle single electron (1e) equivalents among dehydrogenases and the respiratory electron transfer chain of mitochondria and aerobic bacteria (1–3). This activity is mediated by a flavin adenine dinucleotide (FAD) bound in a domain ("head" or "shuttle") that is found in one of two orientations relative to a "base" composed of domains I and III, in crystal structures (4). Naming of ETFs' two subunits and the domains is provided in Figure 1.

In the 1970s, the first report appeared of an ETF containing a second FAD (5), replacing what now appears to be a vestigial adenosine monophosphate (6–8). It has become apparent that diverse anaerobes employ such bifurcating electron transferring flavoproteins (Bf-ETFs) to generate more strongly reducing electron carriers (with lower reduction midpoint potentials, E°s) based on abundant but only modestly reducing nicotinamide adenine dinucleotide (NADH) (9, 10).

"Bifurcation," or more accurately electron transfer bifurcation, captures excess energy released from a favorable electron transfer (ET) to higher E°, by using it to drive an unfavorable transfer (9). The resulting reduced flavodoxin and ferredoxin provide reducing equivalents needed for demanding reactions including nitrogen fixation and carbon fixation (11–13). In brief, a pair of electrons is acquired from NADH by a flavin dubbed the "bifurcating flavin" (^{Bf}flavin) because it passes each of the two electrons to separate acceptors. One electron undergoes exergonic electron transfer *via* the electron transferring flavin (^{ET}flavin), thereby paying for endergonic ET of the second electron to a low-E° acceptor (Fig. 1). To prevent both of NADH's electrons from exploiting the exergonic path, it is critical that the ^{ET}flavin only accept electrons one at a time. In contrast, the ^{Bf}flavin needs to acquire electrons in pairs from NADH. Thus, it might seem surprising that nature has adopted the use of flavins for both roles.

A conformational change is believed to act as a gate, separating the ^{ET}flavin from the ^{Bf}flavin after one electron has been transferred, and thereby enforcing transfer of the other electron to the other acceptor (14, 15). The two conformations seen in crystal structures reveal an 80° rigid-body rotation of the shuttle domain that carries the ^{ET}flavin, removing it from near the ^{Bf}flavin (16, 17) to a position more than 35 Å away and interacting instead with the high-E° acceptor partner protein (4, 14, 15, 18, 19). It remains unclear how this domain movement is coupled to catalytic events and what local perturbations trigger it. However, we note that the high E° determined for reduction of the ^{ET}flavin from the oxidized state (OX) to anionic semiquinone (ASQ) ($E°_{OX/ASQ}$) suggests that ^{ET}flavin will be ASQ in resting enzyme and therefore only capable of accepting one more electron. Thus, the redox tuning applied by the protein environment appears to make the ^{ET}flavin into a 1e acceptor (6, 20, 21).

* For correspondence: Anne-Frances Miller, afmill3r2@gmail.com; Maria-Andrea Mroginski, andrea.mroginski@tu-berlin.de.
Present address for Rajiv K. Kar: Jyoti and Bhupat Mehta School of Health Sciences and Technology, Indian Institute of Technology Guwahati, Assam, India.

Interactions that differentiate Bf-ETF's flavins

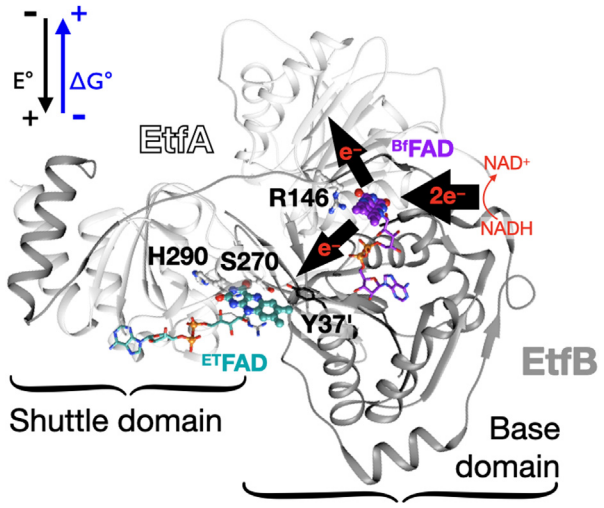

Figure 1. The two FAD-binding sites in the context of the Bf-ETF ribbon structure in the "closed" conformation, based on the crystal structure of *Acidaminococcus fermentans* ETF (*Afe*ETF) (53). An 80° rotation of the shuttle domain produces the "open" conformation (Fig. S1 (14, 15)). The larger EtfA polypeptide is in *light gray*, and the smaller EtfB polypeptide is in *dark gray*. Flavin head groups are in heavy ball-and-stick cartoons with the balance of the FAD and residues of special interest shown as sticks. Residues are numbered according to *Afe*ETF, and those derived from EtfB bear an apostrophe. C atoms are colored *teal* for the ^{ET}flavin and *purple* for the ^{Bf}flavin. All other atoms are colored according to the Corey, Pauling and Koltun (CPK) color convention. Heavy arrows indicate electron transfers involved in bifurcation.

Indeed, we argue that the extreme chemical versatility of flavins has made them invaluable cofactors over the course of evolution, as different proteins can be evolved to emphasize different aspects of the flavin's repertoire by surrounding it with amino acid residues that modify the flavin electronics and accessibility in different ways (22). Thus, biosynthesis of this one cofactor enables cells to satisfy many catalytic needs (23). At issue here, the isoalloxazine core of the flavin is poised between 1e and 2e reactivity by its two 1e E°s that are weakly crossed (9, 24), resulting in predominantly 2e reduction from OX to the 2e reduced hydroquinone (HQ), but with a thermodynamically accessible semiquinone (SQ) state that can be populated to approximately 1% at neutral pH (24). Thus, a protein site able to make relatively modest changes to the relative energies of the OX, SQ, and HQ states can shift the reactivity of the flavin between 1e and 2e transfers. Furthermore, both the SQ and HQ states have physiologically accessible pK_as, of 8.5 and 6.8, respectively (24, 25). Consequently, proteins can modulate local electrostatics to (dis)favor the ASQ or anionic HQ (AHQ) (26), or they can modulate the favorability of proton transfer coupled to ET. Further interventions are achieved *via* orchestrated changes of the local dielectric that can alter the energy associated with a given charge (27). Steric interactions producing distortions characteristic of more reduced states are also expected to raise the flavin E°s (28, 29). In addition, the flavin π system incorporates several functionalities that engage in hydrogen bonds (H-bonds). These provide additional mechanisms by which proteins can tune the reactivity of flavins (Fig. 2). Vibrational spectroscopy reveals that the flavins' two carbonyl O atoms respond to H-bonding, and NMR reveals changes in local electron density distribution as a result of H-bonds to the O and N atoms (30–33).

ETFs appear to employ several of the above features to tune the relative stability of the ^{ET}flavin's ASQ (34–36). A positively charged Arg or Lys adjacent to the ^{ET}flavin is conserved in 98% of Bf-ETFs and has been shown to stabilize the ASQ and impede formation of the AHQ (34–37). Bf-ETFs also conserve a Thr or a Ser near the N5 of the ^{ET}flavin and substitution of this residue affects the E°s (37). In addition, a His near ^{ET}flavin's O2 is conserved in 90% of Bf-ETFs but has not been as well characterized in the literature (statistics are based on an alignment of 228 Bf-ETF sequences (38)). The Bf site also possesses a 99% conserved Arg (otherwise Lys). Unfortunately, its substitution destabilizes the protein and abrogates flavin binding. Therefore, little is known about how it may affect the reactivity of the flavin (34). Moreover, because the ASQ state of ^{Bf}flavin does not normally accumulate in high-quality ETF preparations, it is not possible to study it experimentally to learn how the protein destabilizes it. Thus, computational approaches can fill a critical knowledge gap, elucidating mechanisms of tuning applicable to the ^{Bf}flavin, while using the more accessible ^{ET}flavin as a control for which computations can be validated by experiments (6).

Results

We begin by validating our computational approach (see "Validation: Computational Replication of Contrasting Flavin Reactivities"), then provide a comparative overview of interactions observed in each of the two sites (see "Overview of the Sites' Geometries and Protein–Flavin Interactions"), before describing striking electrostatic differences between them, in the section on "Effect of Protein Electrostatics on Distribution of Electron Density in the Flavins." In the section "Interactions in the ET site," examination of H-bonding in the ET site identifies the interplay between H-bonding at ^{ET}O2, formation of ^{ET}ASQ, and the protonation state of ^{ET}N5, which enables a conserved His at position 290 to influence reactivity at ^{ET}N5. Although the crystallographic Bf site seems considerably less responsive to flavin oxidation state than the ET site, based on our models obtained by energy minimization (see "The Bf Site: H-Bonding at ^{Bf}N5") a model incorporating an alternative rotamer of R146 raises interesting new possibilities (see "H-Bonding by Another Rotamer of R146, for the AHQ of ^{Bf}Flavin") and suggests a basis for the high conservation of this residue.

Validation: computational replication of contrasting flavin reactivities

Before using our models to *explain* the contrasting reactivities of the two flavins, we tested whether they succeed in *reproducing* the differences. In experiments, the ET site stabilizes ^{ET}ASQ, populating this state to 90% during stepwise reductions (39). In contrast, free flavin only accumulates 1% of the population as ASQ, whereas ≥99% undergoes 2e reduction directly from OX to HQ (24). Thus, a favorable ASQ state,

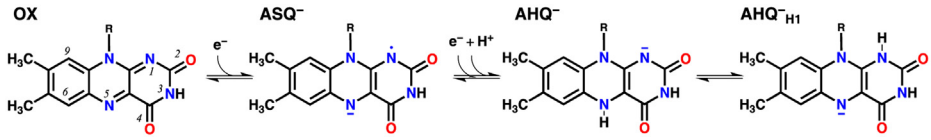

Figure 2. Flavin oxidation states discussed in this study and numbering of key positions in italics (all viewed from the *si* face, numbering shown for OX only). Full numbering is provided in Scheme S1. In the text, H5 denotes the H atom, whereas N5 denotes the N atom, both at the 5 position. R = ribityl adenosine diphosphate for FAD, truncated to -CH_3 in quantum mechanical (QM) calculations. States shown are OX, oxidized; ASQ, anionic semiquinone (1e reduced); AHQ, anionic hydroquinone (2e reduced); AHQ_{H1}, anionic hydroquinone protonated at N1 instead of N5 (2e reduced).

specifically in the ET site, is a critical test of whether our models correctly describe this site. The ET site also makes bound flavin more amenable to reduction than free flavin, whereas the Bf site has the opposite effect (6, 20, 21, 39), so a test of our Bf site models is that they should disfavor flavin reduction.

Our models succeed on both criteria. Based on Gibbs free energy differences (Table 1), formation of ASQ from OX is favorable in the ET site, only. The contrasting computed energy differences clearly stem from the protein, as the two sites produced deviations in opposing directions from the value for gas-phase flavin. Second, formation of AHQ was calculated to be less favorable in the Bf site than in either the ET site or the gas phase, validating our models of that site as well. Although qualitative, these successes are impressive considering the many aspects of protein environments that can contribute to flavin reactivity (see the introduction section), in conjunction with the computational parsimony required to permit the desired characterizations of the numerous states believed to contribute to reactivity.

Because they replicate the different reactivities of the two flavins, our computations provide a basis for evaluating the roles played by different aspects of the protein environment. Here we have considered local electrostatics, geometry imposed by the protein, and H-bonds. Such factorization is difficult in experiments, where residue substitutions tend to change all three contributions at once.

Overview of the sites' geometries and protein–flavin interactions

Our computations reveal interplay between each flavin and protein residues nearby, as summarized in Figure 3. H-bonding with flavin positions N3 and O4 was found to be mainly with protein backbone carbonyl (=O) and amide (NH) groups and therefore could be coupled to higher-order structure. However H-bonds to flavin O2 were also provided by side chains or a water molecule, which can be more mobile. H-bond donation to flavin N5 was also *via* amino acid side chains in both sites, which is significant because the 5 position is converted from an H-bond *acceptor* to an H-bond *donor* upon acquisition of a proton as part of reduction to form AHQ (Fig. 2). Thus, ETF's presentation of side chains to that position obviates a need for the backbone reorientation seen in flavodoxin (40). In both sites, reorientation of the side chain interacting at N5 enabled the protein to accept an H-bond from the flavin AHQ, where it had donated one to OX and ASQ (see sections on "Interactions in the ET site" and "The Bf site: H-bonding at ^{Bf}N5").

Reduction of ^{ET}flavin to ^{ET}AHQ caused the side chains of S270 and Q266 to reorient, reversing the polarities of their interactions with the ^{ET}flavin. In addition, a segment of backbone at G271 relinquished its H-bond to ^{ET}O4 and moved away by 1 Å (Fig. 4*A*). Thus, the protein constituents of our computed ET site are conformationally responsive to the oxidation state of ^{ET}flavin and not frozen in the ^{ET}OX crystal structure. Our computations thus suggest that the ET site supports facile ^{ET}flavin reduction via provision of a highly fluid or adaptive network of H-bonds from mobile side chains and backbone loops.

Table 1
Gibbs free energy differences between flavin oxidation states in each of the binding sites of *Afe*ETF[a,b]

	ΔG [kcal/mol]	
Flavin's environment	ASQ - OX	AHQ - OX
Gas phase LF	−36	−408
^{Bf}flavin	4	−352
^{ET}flavin$_\delta$	−73	−385
^{ET}flavin$_\varepsilon$	−73	−388

[a] For the protein-bound flavins, the protein environment was represented as a distribution of electrostatic point charges. Comparisons can be made only within individual columns. The large difference between the sets of energies associated with each of the two chemical events may reflect our neglect of intrinsic energies of the electrons and proton that feature in the balanced equations for the different reductions.
[b] For completeness, corresponding electronic energy differences are given in Table S1.

Effect of protein electrostatics on distribution of electron density in the flavins

Electrostatic stabilization of the different flavin oxidation states by each of the protein sites was assessed *via* computation of Natural Bond Order (NBO) electron densities (41). Figure 5 shows how the NBO densities deviated from what occurs if the flavin is considered in gas phase but frozen in the geometries produced by the corresponding protein site.

All oxidation states of the ^{Bf}flavin showed greater charge displacements compared with the ^{ET}flavin. In ^{Bf}flavin, position ^{Bf}N5 especially, followed by ^{Bf}O4, ^{Bf}O2, ^{Bf}C6, and ^{Bf}C9, differed from free flavin with the same geometry. It is fascinating that (1) two unsubstituted aromatic Cs were significantly affected (^{Bf}C6 and ^{Bf}C9) and (2) the largest effects were on electronegative atoms, but of these, ^{Bf}N1 and ^{Bf}O2 were net electron depleted while ^{Bf}O4 and ^{Bf}N5 were enriched. A pattern that emerges is that atoms along the "top" edge as displayed (^{Bf}C9, ^{Bf}C10, ^{Bf}C1′, ^{Bf}N1, ^{Bf}O2) were rendered electron deficient by the Bf site but not the ET site. We speculate that this reflects electrostatic repulsion by the pyrophosphate of the ^{Bf}FAD

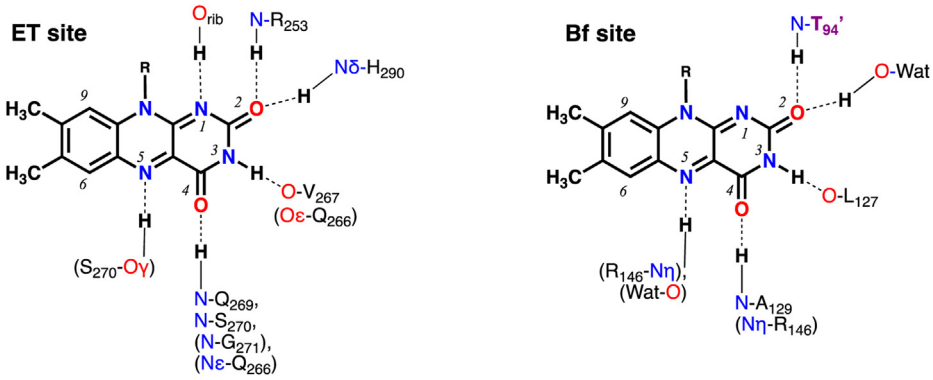

Figure 3. Residues that interact with the ^{ET}flavin and the ^{Bf}flavin. Flavins are viewed from the *si* face and portrayed in their OX states. Weak interactions or interactions specific to particular oxidation states are in parentheses, see text for details. T94′ (in *purple*) resides in EtfB monomer whereas all other residues specified in this scheme derive from EtfA. The H-bond to N1 of the ^{ET}flavin derives from the ^{ET}FAD's own ribityl chain (48). Amino acid side chain atoms bear Greek specifiers whereas the backbone amide N and H and the backbone carbonyl O do not. This convention will be used throughout.

because the kinked conformation of the ^{Bf}FAD's ribose places the phosphates less than 6 Å from the top edge of the ^{Bf}flavin (Fig. 1), whereas the ^{ET}FAD is more extended.

The ET site produced completely different effects on NBO density, barely perturbing excess electron density distribution in ^{ET}OX, compared with gas phase. This is consistent with ^{ET}flavin's greater solvent accessibility in Bf-ETF of *Acidaminococcus fermentans* (*Afe*ETF) (34). However, in ^{ET}ASQ, the ^{ET}N1 position bore much more excess electron density, as did ^{ET}O2. Among the heteroatoms, the only position to bear more positive charge relative to that seen for gas-phase flavin was ^{ET}N3H (sum of NBO charges of ^{ET}N3 and ^{ET}H3), in further contrast with ^{Bf}flavin. This concentration of negative charge on electronegative ^{ET}N1 and ^{ET}O2 was specific to the ^{ET}ASQ state and is chemically favorable, suggesting a basis for the unique stability of ^{ET}ASQ. However, it is not easy to explain based on charged residues nearby. The only charged side chain within 7 Å of ^{ET}flavin is that of R253, and its guanidinium functionality is closer to the flavin xylene ring than to ^{ET}O2 and ^{ET}N1.

Interactions in the ET site

To understand migration of electron density to ^{ET}O2, we investigated H-bonds nearby. His290 is conserved in 90% of Bf-ETF sequences, so we tested the possible significance of an H-bond by modeling H290 in two tautomers. The δ-tautomer bearing an H on the δN could donate an H-bond to ^{ET}O2 but the ε-tautomer bearing an H on the εN instead could not, based on the energy minimized structures (Fig. 6). Indeed, Figure 5 shows that strong excess electron density on ^{ET}O2 was specific to the δ tautomer, indicating that H-bond donation from H290 is responsible.

If an H-bond is to tune an E° of ^{ET}flavin, it must change the energy of one oxidation state more than that of the other state. This is a result of the direct proportionality between E° and the free energy change upon reduction. For the example of reduction of OX to ASQ, $E^{\circ}_{OX/ASQ} = -(G^{\circ}_{ASQ} - G^{\circ}_{OX})/nF$, where F is Faraday's constant, n is the number of electron equivalents acquired and n = 1 in this case. If an H-bond lowers the free energy of the ASQ state more than the free energy of the OX state, then the quantity inside the parentheses becomes more negative and the right side of the equation becomes more positive (F is positive). Thus, the new $E^{\circ}_{OX/ASQ(Hbd)}$ modified by H-bonding becomes more positive. This is illustrated in supporting Fig. S2. Because a stronger (shorter) H-bond lowers a state's energy more than a weaker (longer) one, the foregoing example would correspond to a shorter H-bond in the ASQ state than in the OX state.

H-bond strengths were therefore assessed, *via* the proxy of their lengths, and compared for all three observed oxidation states (Tables S6–S8). In the ET site, some H-bond lengths

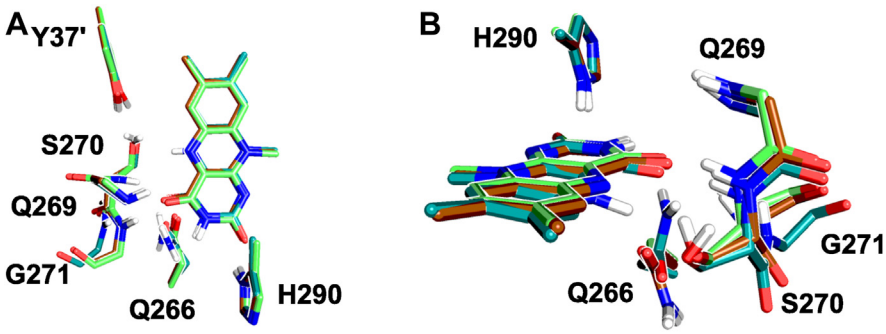

Figure 4. Overlay of ^{ET}OX$_{\delta}$, ^{ET}ASQ$_{\delta}$, ^{ET}AHQ$_{\delta}$. The ^{ET}flavin is viewed from the *si* face (*A*) and from the xylene ring end (*B*) with the energy-minimized structure of ^{ET}OX in *brown*, that of ^{ET}ASQ in *light green*, and that of ^{ET}AHQ in *darker teal*. The lowest-energy structures are shown, corresponding to the second energy minimum of ^{ET}AHQ as described below. *A* shows the displacement of backbone near G271 upon reduction to the ^{ET}AHQ state (*lower left of panel*). The same displacement is evident in the *lower right* of *B* in the orientation of S270's backbone O.

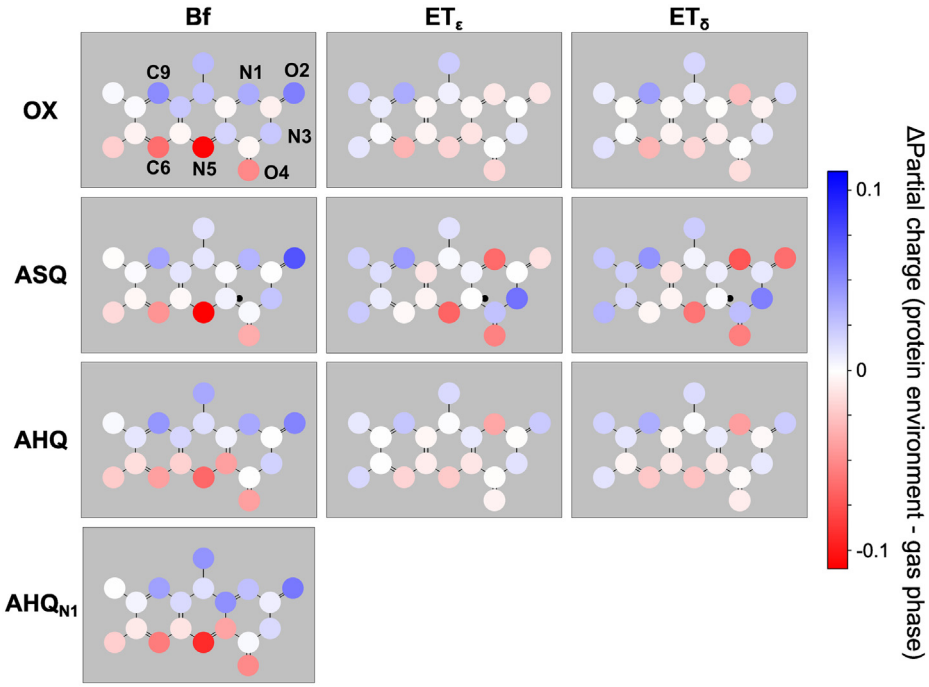

Figure 5. Flavin ring structures with positions color coded by differences in the NBO partial charges produced by the protein electrostatic environment. The flavin geometries were held constant as optimized in the protein QM/MM, and the protein environment was provided in the form of the partial charges of the protein atoms. To emphasize the effect of protein electrostatics, differences plotted are "in presence of protein charges" minus "in absence of protein charges" with the same flavin geometry (a.k.a. "frozen gas phase"). Hydrogen charges were added to those of the heavy atoms to which they are bound. Partial charge values are shown in Tables S2–S5.

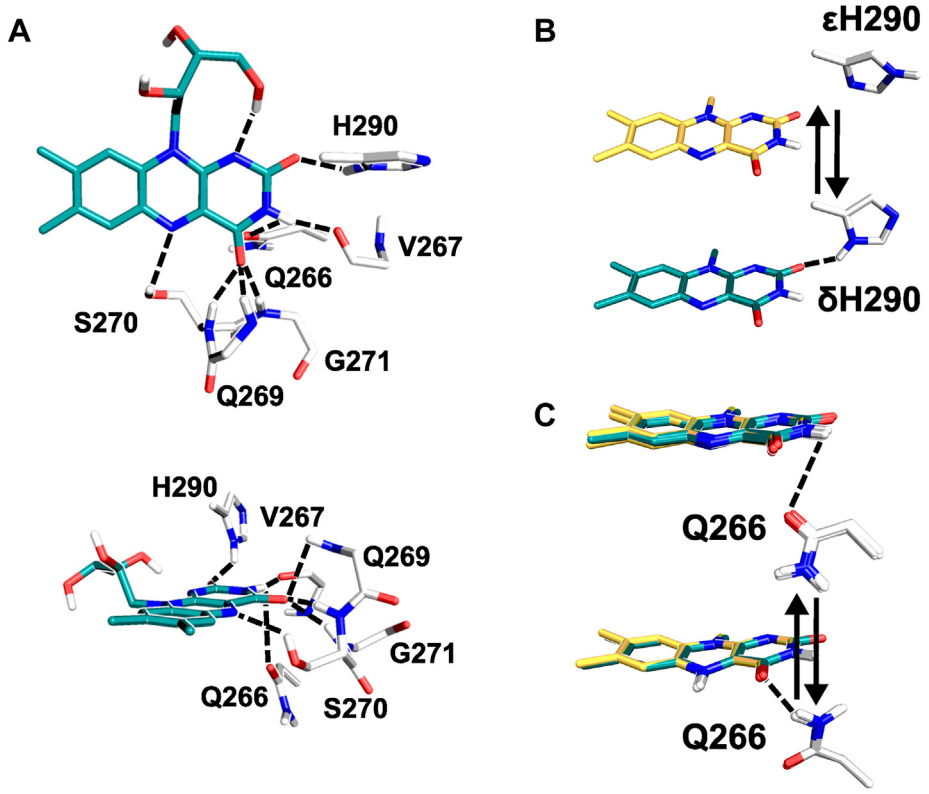

Figure 6. Interactions responsive to ^{ET}flavin's oxidation state. *A*, H-bond network for $^{ET}OX_\delta$ viewed from the *si* face (*top*) or edge-on with the xylene ring in front and the uracil ring behind (*below*). *B*, Tautomers of H290 present in $^{ET}OX_\varepsilon$ (*top*, *yellow* C atoms in flavin) and $^{ET}OX_\delta$ (*below*, *teal* C atoms for flavin). *C*, Conformations of Q266 produced by energy minimization of ^{ET}OX or ^{ET}ASQ (*top*) *versus* the conformation of Q266 produced by energy minimization of ^{ET}AHQ (*below*) (*yellow* ^{ET}flavin$_\varepsilon$ and *teal* ^{ET}flavin$_\delta$).

were relatively invariant (changes ≤ 0.2 Å in donor–acceptor distances (42)). However, four underwent qualitative change, being engaged only in certain oxidation state(s) (Table S8). These included the H-bond between ^{ET}O2 and H290 whose H moves into H-bonding position between the two heavy atoms only in the ^{ET}ASQ state (Fig. 6*B*). Additional responsive H-bonds were from backbone to ^{ET}O4 (Fig. 6*A*), a weak H-bond from the side chain of Q266 to ^{ET}O4 that is exclusive to the AHQ state (Fig. 6*C*), and the interaction between ^{ET}N5 and the side chain of S270 that reverses polarity upon formation of ^{ET}AHQ (with acquisition of the ^{ET}H5 proton, Fig. 6*A*).

H-bonds involving the backbone are of particular interest, because repositioning of backbone could trigger changes in the protein secondary and higher-order structure. In the ET site, the backbone HN of G271 H-bonded to ^{ET}O4 in ^{ET}OX and ^{ET}ASQ but was released upon formation of ^{ET}AHQ. The ^{ET}O4–N distance increased from 3.0 to 3.9 Å in ^{ET}AHQ$_\delta$ and from 3.1 Å to 4.0 Å in ^{ET}AHQ$_\varepsilon$. Detachment of G271 was coupled to rotation of the side chain of Q266, which changed from being a recipient from ^{ET}H3 of ^{ET}OX or ^{ET}ASQ to being an H-bond donor to ^{ET}O4 of ^{ET}AHQ (see Fig. 4). Although these interactions with ^{ET}flavin were weak, the unambiguous rotation of Q266's side chain confirmed distinct and adaptive interactions in the different oxidation states.

Similar redox-coupled rotations of H-bonding Gln side chains have been noted in other flavoproteins, such as BLUF (43, 44). Since gas-phase calculations indicated that the charge density at ^{ET}N3 changes relatively little upon reduction of the flavin but that ^{ET}O4 becomes considerably more negative, especially upon reduction to ^{ET}AHQ (Fig. S3), we speculate that this change corresponds to recruitment of the Q266 amide by ^{ET}O4. The effect would be to stabilize ^{ET}AHQ, consistent with the ^{ET}flavin's relatively high $E^\circ_{OX/AHQ}$ (34).

Although H-bond donation mediated by ^{ET}H5 is possible only in the ^{ET}AHQ state, acceptance at ^{ET}N5 can be compared among all three oxidation states. By comparing an H-bond's length across states we can determine whether the H-bond is stronger (more stabilizing) in one state than the other. An H-bond that is stronger in the reduced state will favor reduction and raise E° (also see Fig. S2). We employed an expanded quantum mechanical (QM) region including S270's side chain in relaxed energy scans of the distance between ^{ET}N5 and the H-bonding H, to compare energy profiles in each oxidation state. In the absence of an H-bond to ^{ET}O2, the energy landscapes were dominated by a single geometry with a well-defined but long optimal H-to-^{ET}N5 distance (yellow curves in Fig. 7, optimal distance values are provided above each profile for the system with the δ tautomer of H290). Energies associated with H-to-^{ET}N5 distances exceeding 2.1 Å are likely small (45, 46) and were not considered to constitute an H-bond (47). For reference, distances on the order of 1.7 ±0.1 Å were obtained between the H-bonding H and the accepting O atom in work on rhodopsin (45). Interestingly, several profiles revealed that more than one configuration of interactions can produce a stable minimum. These occurred when ^{ET}N5 was protonated (Fig. 7*B*) or when ^{ET}O2 received an H-bond, despite the spatial separation of these two interactions. The associated structures revealed a network of interacting residues surrounding ^{ET}N5 and ^{ET}H5 (Fig. S4). Thus, the observed stabilization is the result of numerous weak interactions rather than a single strong one.

We also characterized H-bonding at ^{ET}O2 because receipt of an H-bond at ^{ET}O2 enabled stable second minima, similar to acquisition of a proton at ^{ET}N5 (Fig. 7*B*). To test for participation in redox tuning, we profiled H-bond acceptance strength *versus* oxidation state by scanning along ^{ET}O2's H-bond in the three oxidation states with the δ tautomer of H290 (Fig. 8). In the event of negative cooperativity between protonation at ^{ET}N5 and ^{ET}O2 H-bond acceptance, we expect a longer optimal H-bond to ^{ET}O2 in ^{ET}AHQ$_\delta$ (protonated at ^{ET}N5) than in ^{ET}ASQ$_\delta$, despite their identical total charges. Computations confirmed this, as well as a broader energy landscape in the ^{ET}AHQ$_\delta$ state where protonation of ^{ET}N5 limits electron density migration to ^{ET}O2 (Fig. 5).

In contrast, the tighter potential well for the ^{ET}ASQ$_\delta$ state (Fig. 8*B*) reinforces the evidence of charge distribution and the lower energy of ^{ET}ASQ$_\delta$ *versus* ^{ET}ASQ$_\varepsilon$ that there is a favorable synergy between the ^{ET}ASQ state and H-bonding to ^{ET}O2. The shorter O2–^{His}Hδ distance of 1.9 Å in the ASQ state compared with 2.5 Å in the OX state confirms a significantly stronger H-bond to O2 in the ^{ET}ASQ than in ^{ET}OX consistent with stabilization of ^{ET}ASQ relative to ^{ET}OX by this interaction, and hence elevation of $^{ET}E^\circ_{OX/ASQ}$. Thus, we find that the H-bond to ^{ET}O2 is an important contributor to ^{ET}flavin's unusually stable ASQ state.

The Bf site: H-bonding at ^{Bf}N5

The energy-minimized Bf site structures seemed less responsive to oxidation state changes than those of the ET site (Tables S8 and S10). In addition, the Bf site did not donate an H-bond to N1, one of the interactions that may stabilize ASQ in the ET site (see Fig. 3) (48). The ET site displayed a constellation of backbone NHs donating H-bonds to O4, whereas the energy-minimized Bf site provided only one weak H-mediated interaction (≥3.4 Å from A129 amide N to ^{Bf}O4, ≥ 2.4 Å from H to ^{Bf}O4). Thus, states and positions with more electron density appear poorly stabilized by H-bonds to the ^{Bf}flavin, consistent with its less favorable reduction than ^{ET}flavin (Table 1). However, ^{Bf}OX may be better stabilized, as the distance between ^{Bf}flavin's N5 and the H-bond donating heavy atom was shorter in ^{Bf}OX (2.9 Å) than in the ^{ET}OX$_\delta$ and ^{ET}OX$_\varepsilon$ models (3.3 and 3.3 Å). This distinction could be a contributor to ^{Bf}flavin's lower E°, so we investigated further.

Relaxed scans of the H-bond between R146 and ^{Bf}N5 suggested a weak tendency for ^{Bf}ASQ's N5 to capture a proton from R146, although that structure was high in energy and corresponds to the saddle point at an H-to-^{Bf}N5 distance of 1 Å rather than a genuine local minimum (Fig. 9*B*). We therefore tested the possibility of proton transfer from R146 to ^{Bf}N5 in the other anionic oxidation state, by comparing ^{Bf}AHQ protonated at N5 (the default) with the ^{Bf}AHQ$_{H1}$ tautomer (see Fig. 2). In this case, a defined local minimum was obtained

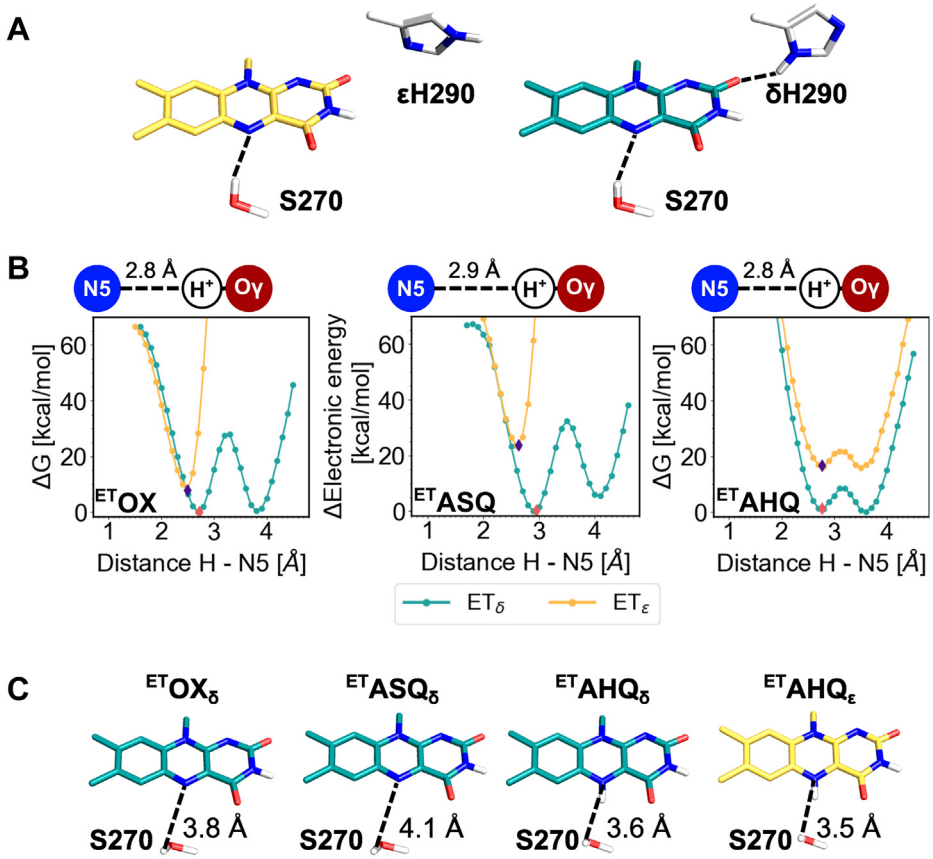

Figure 7. Relaxed energy scans of the interaction with ^{ET}N5 in the different states of the ET site. *A*, the H-to-N5 distance from S270's Hγ to the ^{ET}flavin that was scanned, shown in the presence of each of the H290 tautomers tested. *B*, scans of the Hγ-to-^{ET}N5 distance between S270 and ^{ET}N5. Some of the systems displayed a second energy minimum at longer Hγ-to-^{ET}N5 distance. *C*, ^{ET}flavin and S270 geometries for the second energy minima. The energy difference between $^{ET}OX_\varepsilon$ and $^{ET}OX_\delta$ was ε-δ = 7.8 kcal/mol, for $^{ET}ASQ_\varepsilon$ and $^{ET}ASQ_\delta$ it was 23.4 kcal/mol, and for $^{ET}AHQ_\varepsilon$ and $^{ET}AHQ_\delta$ it was 16 kcal/mol. In addition, the energy differences between the first and second local minima (first minimum minus second minimum) were −0.4 kcal/mol ($^{ET}OX_\delta$), −5.5 kcal/mol ($^{ET}ASQ_\delta$), 1.1 kcal/mol ($^{ET}AHQ_\delta$), and 0.5 kcal/mol ($^{ET}AHQ_\varepsilon$). Positive energy differences indicate that the newly discovered local energy minimum is more stable than the starting geometry (values in bold), and therefore that any H-bond to ^{ET}AHQ from S270 appears to dissociate in the ^{ET}AHQ state, confirming expected behavior.

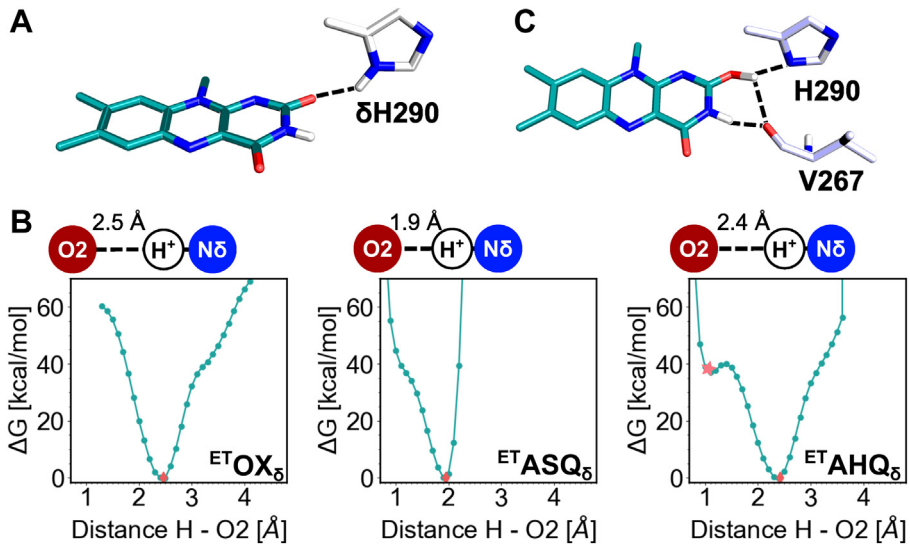

Figure 8. Relaxed energy scans along the ^{ET}O2 H-bond of ^{ET}flavin for the δH290 systems. *A*, H-bond scanned. *B*, scans of H-bond donated to ET FAD's O2 by δH290. *C*, structure corresponding to the local energy minimum that appeared at shorter H-bond distances in the $^{ET}AHQ_\delta$ state, indicating proton transfer to the ^{ET}flavin's O2 atom. However, the local energy minimum was almost 40 kcal/mol higher than the global minimum obtained, corresponding to a negligible Boltzmann population for this state.

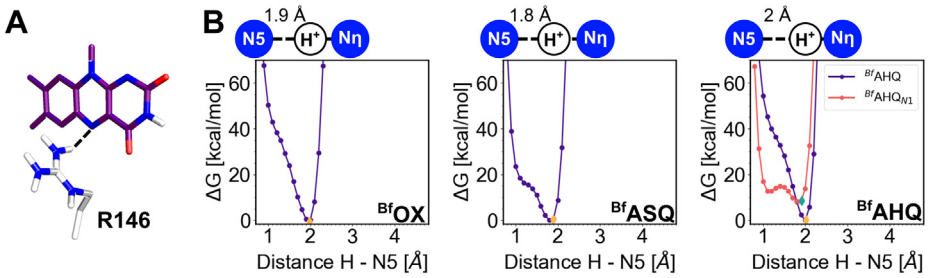

Figure 9. Energy profiles of the H-bond donated to ^{Bf}N5 as a function of ^{Bf}flavin's oxidation state. *A*, H-bond scanned in the ^{Bf}flavin site. *B*, scans of H-bond between R146 and ^{Bf}N5, showing weak inflection points at distances shorter than optimum. In the right pannel, the *purple curve* and associated points describe ^{Bf}AHQ protonated at N5, whereas the *coral pink curve* and associated points describe the AHQ tautomer protonated at N1 instead, ^{Bf}AHQ$_{H1}$, see Figure 2 for structures. The free energy difference between the two minima of ^{Bf}AHQ$_{H1}$ was 4.6 kcal/mol. The free energy difference between the ^{Bf}AHQ$_{H1}$ minimum and the N5-protonated ^{Bf}AHQ minimum was 8.2 kcal/mol.

with a shorter H-to-^{Bf}N5 distance that corresponds to proton transfer from R146 to generate neutral HQ (Fig. 9*B*). Given the 12.8 kcal/mol higher energy of this conformation compared with that of the default ^{Bf}AHQ, it appears that the neutral HQ would only be populated to 3.8×10^{-10} (corresponding to a pK_a ≈ 2.4). However, it could serve as a transition state in catalysis, for example, mediating proton transfer to/from ^{Bf}N5 where the proton would be acquired from NADH.

H-bonding by another rotamer of R146, for the AHQ of ^{Bf}flavin

Although our energy-minimized ^{Bf}AHQ system was protonated at N5, no potential H-bond acceptor for H5 was observed following simple geometry optimization starting from the OX state crystallographic protein geometry. Instead, the H5 of ^{Bf}AHQ was directed at the side chain of the conserved Ile157. This, and the flavin's retention of almost flat geometry in the AHQ state (Fig. S5), raised concern that our energy-minimized ^{Bf}AHQ might not describe the global energy minimum. To test for additional low-energy conformations of the AHQ Bf site, we surveyed all possible rotamers of R146. Most were excluded on steric grounds, but two formed favorable H-bonds with ^{Bf}flavin. After the standard energy minimization and QM/molecular mechanical (MM) optimization, a conformation was obtained with a Gibbs free energy only 1 kcal/mol above that of the crystal structure-derived model ^{Bf}AHQ (Table S11). We therefore assessed this structure as an alternative model for the ^{Bf}AHQ state, ^{Bf}AHQ$_{R146}$, and henceforth refer to the OX crystal structure-derived models as ^{Bf}AHQ$_{xtal}$. The stability of the alternative conformation seems specific to the AHQ state as OX$_{R146}$ and ASQ$_{R146}$ models obtained by energy minimization starting from ^{Bf}AHQ$_{R146}$ with OX or ASQ flavin yielded significantly higher Gibbs free energies compared with the corresponding ^{Bf}OX$_{xtal}$ and ^{Bf}ASQ$_{xtal}$ models. Therefore, only ^{Bf}AHQ$_{R146}$ was pursued. The finding that this conformation stabilizes specifically the AHQ state makes it an additional possible contributor to redox tuning.

^{Bf}AHQ$_{R146}$ differed from ^{Bf}AHQ$_{xtal}$ by reorientation of the R146 side chain to donate an H-bond to the ^{Bf}O4 *via* the *re* face, as opposed its H-bond donated from the *si* face to ^{Bf}N5 in the ^{Bf}OX$_{xtal}$ structure (Fig. 10). A water took the position vacated by R146 and became an H-bond acceptor from ^{Bf}H5. This greatly improves the site's compatibility with the ^{Bf}AHQ, because N5H is a poor acceptor but a good H-bond donor *via* H5. Moreover, the new water near ^{Bf}H5 is a much better H-bond acceptor than the side chain of I157. These can explain why the ^{Bf}AHQ$_{R146}$ model becomes competitive specifically in the AHQ state.

Reorientation of R146's side chain also resulted in a new H-bond from it to ^{Bf}O4 (Fig. 10). This joined the H-mediated interaction from the backbone NH of A129 (Fig. 10*A*). However, the new H-bond from R146's side chain was stronger than that from A129, based on a distance of 2.7 Å between R146's Nη1 and ^{Bf}O4 (*versus* 3.0 Å from A129-N to ^{Bf}O4, Table S12 and Fig. S6), consistent with R146's positive charge and more labile Hη1 *versus* the backbone amide NH of A129. This new stronger H-bond can explain the greater negative charge that accumulated at ^{Bf}O4 upon formation of flavin ^{Bf}AHQ$_{R146}$, compared with ^{Bf}AHQ$_{xtal}$ (Fig. 11 and Fig. S8). In turn, the greater charge density at ^{Bf}O4 makes sense of A129's H-bond to ^{Bf}O4 being shorter (stronger) in ^{Bf}AHQ$_{R146}$ where it shares ^{Bf}O4 with R146, than in ^{Bf}AHQ$_{xtal}$. H-bond contractions were also indicated at ^{Bf}O2 and ^{Bf}N3H as well, albeit small ones. Thus, R146's reorientation and recruitment of a better H-bond acceptor for ^{Bf}N5H appear to produce a generally more favorable complex in ^{Bf}AHQ$_{R146}$, based on geometrical and electrostatic criteria.

Finally, the ^{Bf}AHQ$_{R146}$ model escaped the perplexing OX-like geometry retained by the ^{Bf}AHQ$_{xtal}$ model. ^{Bf}AHQ$_{R146}$ deviated considerably from planarity (Figs. 10*A* and 11*C*), in agreement with structural studies of numerous other reduced flavin sites (28, 29, 49). Thus the ^{Bf}AHQ$_{R146}$ model provides a chemically and energetically plausible additional conformation to describe the AHQ state of the Bf site.

Discussion

Beginning with the crystal structure of OX *Afe*ETF, we examined the effect of placing the flavin in each of the three oxidation states known for this system, for each of the two flavins. To generate optimized sites, we used MM energy minimization followed by QM/MM geometry optimization treating the flavin quantum mechanically and relaxing residues with any atom within 5 Å. Despite its simplicity, this protocol documented reorientation of a side chain, 1 Å repositioning of

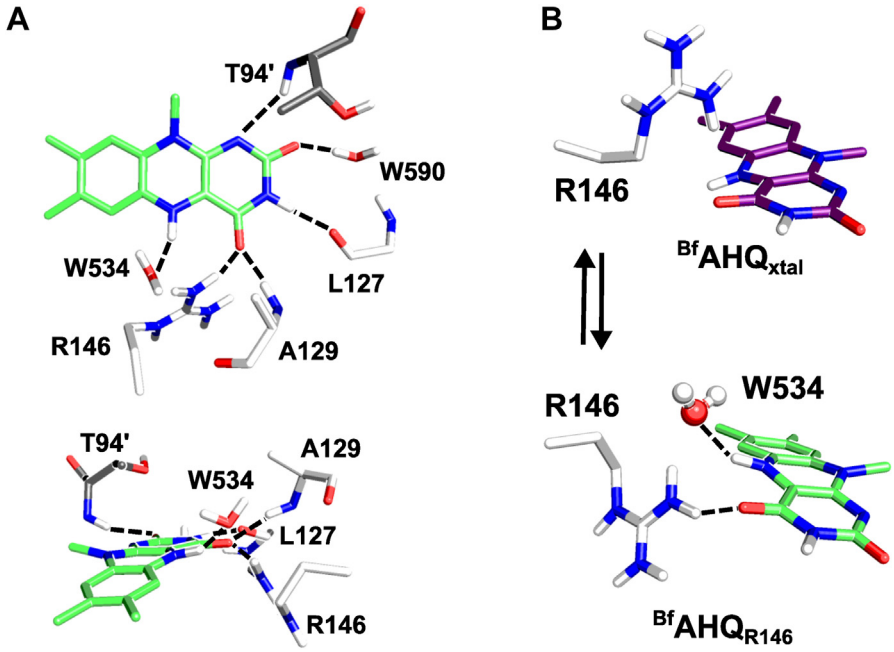

Figure 10. Hydrogen bonding with ^{Bf}flavin in the AHQ$_{R146}$ model. *A*, H-bond network in the ^{Bf}AHQ$_{R146}$ model viewed from the *si* face (*top*) *versus* edge-on view of the flavin showing its bent geometry and H-bonding involving R146 (*below*). *B*, comparison of the rotamers of R146 present in ^{Bf}AHQ$_{R146}$ (*green flavin*) and ^{Bf}AHQ$_{xtal}$ models (*purple flavin*, as in Fig. 9).

a loop of backbone and reorganization of a critical H-bonding network supporting the redox-active N5 (37), for the ET site. The Bf site did not adapt in the course of energy minimization when different oxidation states of the flavin were embedded in it. However, a screen of alternative rotamers for side chains able to H-bond with the ^{Bf}flavin revealed an additional energetically viable conformation. For both sites, H-bonds of interest were characterized *via* constrained variation of the lengths of H-bonds donated to N5, in each flavin oxidation state, with the H-bond donor included in the quantum regime. This protocol yielded profiles of energy *versus* H-bond length that identify H-bonds related to redox tuning. Our studies revealed three overarching distinctions between the two flavin sites that suggest explanations for their contrasting reactivities.

Adaptive network of H-mediated interactions surrounding N5 in the ET site

The ET site has a highly adaptive network of multiple weak interactions supporting ^{ET}N5 and accommodating its acquisition of ^{ET}H5, whereas the Bf site resisted redox-coupled change. This may suppress the ^{Bf}ASQ state in so far as reduction by only one equivalent may not suffice to drive any conformational change needed to stabilize reduced ^{Bf}flavin. Full reduction and protonation of ^{Bf}flavin may be required to elicit conformational accommodation by this site, where several important H-bonds derive from the backbone (T94′-^{Bf}O2, L127-^{Bf}N3H, A129-^{Bf}O4).

As part of the ET site's adaptive response, the side chain of Q266 reoriented during energy minimization in ^{ET}AHQ. This reversed orientation of the corresponding Gln was recently reported in the crystal structure of lactate dehydrogenase's confurcating ETF (7QH2.pdb (16)), although we caution that the protein database contains several instances of Gln and Asn side chains whose orientations appear to have escaped scrutiny. H-mediated interactions at ^{ET}N5 were weak based on their lengths, but the conformation with the shorter S270–^{ET}N5 distance attained greater significance relative to the second energy minimum, becoming better defined, in the ^{ET}ASQ state. This is consistent with the observed depression of the $E^{\circ}_{OX/ASQ}$ of ^{ET}flavin upon replacement of the residue analogous to S270 (37).

In contrast, geometry optimization of Bf site models did not cause significant displacements. We propose that this reflects considerably steeper energy barriers to reorganization in the Bf site, rather than absence of other local energy minima, since a plausible alternative conformation was identified. An expanded approach including heating and annealing, and/or full molecular dynamics, is needed to sample the conformational space.

Indeed, we have shown that ^{Bf}flavin's AHQ state can favorably engage R146 in a conformation different from that seen in ^{Bf}AHQ$_{xtal}$. Migration of R146 from donating an H-bond to N5 in ^{Bf}OX and ^{Bf}ASQ to donating to ^{Bf}O4 of ^{Bf}AHQ is consistent with the chemical nature of Arg's side chain, which constrains it to always donate an H-bond. In contrast, the N5 of flavin changes from being an H-bond acceptor in the OX and ASQ states to a donor in AHQ, prompting reorganization of H-bonding partners. For ^{ET}flavin this was accomplished by S270 changing allegiance from being a donor to ^{ET}N5 to donating to Y37′ instead, while *accepting* an H-bond donated by ^{ET}H5. In the Bf site, the ^{Bf}AHQ$_{R146}$ model allows R146 to continue to stabilize the anionic ^{Bf}flavin's net charge *via* H-bond donation to ^{Bf}O4, even when ^{Bf}N5 is protonated.

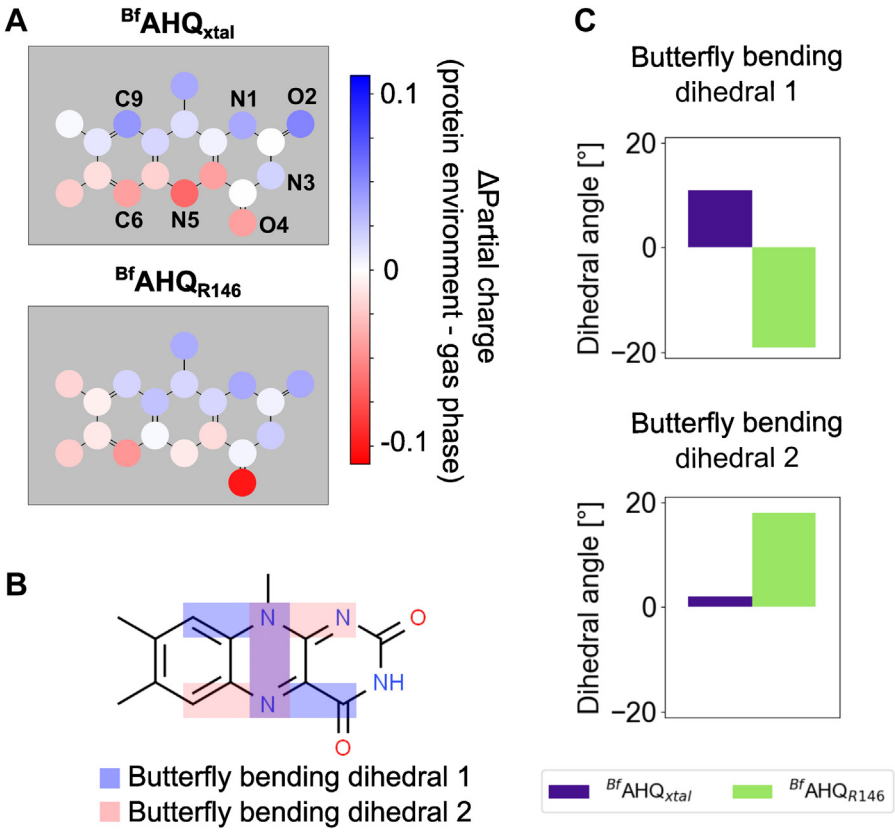

Figure 11. Analysis of steric and electrostatic effects of protein environment on ^{Bf}FAD comparing the crystal structure–derived model ^{Bf}AHQ$_{xtal}$ with ^{Bf}AHQ$_{R146}$. *A*, isoalloxazine color coded by charge difference between protein electrostatic environment and frozen gas phase. *B*, dihedral angles used to quantify the butterfly bending. *C*, bar plots of the dihedral angles comparing the butterfly bending of ^{Bf}AHQ$_{xtal}$ with ^{Bf}AHQ$_{R146}$.

We speculate that an alternative rotamer of R146 may also explain ^{Bf}ASQ stabilization in response to perturbations such as depletion of ^{ET}FAD (50). Furthermore, if R146's conformation is responsive to events in the shuttle domain where ^{ET}flavin resides, then the reverse would also be true and adoption of the ^{Bf}AHQ$_{R146}$ rotamer could contribute to a conformational response on the part of the shuttle domain. Indeed, R146 is modeled in a variety of distinct rotamers among crystal structures of Bf-ETFs (Fig. S7).

Coupling to domain-scale conformation?

The fact that multiple configurations of H-bonding with ^{ET}N5 have comparable energies appears to reflect an underlying network of H-bonds including the side chain of Y37′ as well as the S270 we investigated (Fig. S4). Interestingly, Y37′ resides in the other subunit of *Afe*ETF, in the base domain, whereas ^{ET}flavin is bound in the shuttle domain (Figs. 1 and S1). Only the closed conformation of *Afe*ETF shown in Figure 1 permits H-bonding between S270 and Y37′ as they are separated by more than 20 Å in the open conformation (Fig. S1 (14, 15)). Thus, the Y37′–S270–^{ET}N5 network could modulate the relative energies of the two conformations of *Afe*ETF in response to ^{ET}flavin's oxidation state. The domain scale alternation of conformations is observed even for canonical ETFs that lack a ^{Bf}flavin, consistent with triggering events emanating from the ET site. We also note that depletion of the ^{ET}flavin leads to a change in the redox reactivity of the ^{Bf}flavin (50), confirming mutational evidence that events in one site can affect the other (34). The current local energy minimizations cannot address such long-range effects but can identify local changes that could trigger them. Thus, the reorientation of Q266 upon reduction of ^{ET}flavin is noteworthy. Importantly, the 1-Å shift seen in G271's backbone upon ^{ET}flavin reduction may also be significant to the conformational change, because G271 resides in a loop that forms part of the shuttle domain's interface with the base.

H-bond from His to ^{ET}flavin O2 may stabilize ASQ and support 1e reactivity

We demonstrated that a conserved His in the ET site donates an H-bond to the flavin ^{ET}O2 and stabilizes excess negative charge there, especially in the ^{ET}ASQ state. We tested the significance of this H-bond, *via* comparison of models containing the δ-tautomer of H290, which forms the H-bond, *versus* models containing the ε-H290 and retaining all the same atoms but no H-bond between H290 and ^{ET}O2. Such targeted tests are rarely possible in experiments, highlighting the value of computations (but see (51)). The significance of this H-bond is nevertheless supported by the experiments of evolution, as H290 is 90% conserved and so is the Y279 that supports it. Crucially, Y279 is expected to be protonated at neutral pH and therefore to be an H-bond donor to H290. This

in turn will polarize H290, defining it as an acceptor from Y279 and therefore a donor to ^{ET}O2.

Because ^{ET}O2 is *para* to ^{ET}N5, it has considerable inductive influence over the redox-active ^{ET}N5(H). In δ-His290 systems, the shorter and longer interactions between S270 and ^{ET}N5 were comparably favorable in ^{ET}OX and ^{ET}AHQ (Fig. 7*C*). This is consistent with a shift of excess negative charge to ^{ET}O2 from ^{ET}N5, making the shorter-distance energy well at ^{ET}N5 less deep. The potency of O2's remote effect on N5 reflects the OX state's highly correlated electronic structure (52).

A comparable interaction was not seen in the Bf site, where ^{Bf}O2 H-bonds with a molecule of water in the crystal structure of *Afe*ETF. Water is more likely to adapt to demands made by the flavin than to impose constraints upon it, since water can reorient and reposition to minimize strain. Nevertheless, that water molecule appears to H-bond to the side chain of D93′, which is 100% conserved (in a set of 228 group II Bf-ETF nonbasal sequences (38)). This will make the water a poor H-bond donor to ^{Bf}O2, rationalizing the deficit of electron density on ^{Bf}flavin's ^{Bf}O2 revealed by our NBO calculations in all three oxidation states (Fig. 5). We propose that poor H-bond donation to ^{Bf}O2 contributes to the Bf site's suppression of ^{Bf}ASQ. In addition, although R146 donates an H-bond to ^{Bf}N5 that might be thought to stabilize ^{Bf}ASQ on electrostatic grounds, it concentrates excess electron density on ^{Bf}N5 (Fig. 6) creating a deficit at ^{Bf}O2 that is not favorable, given the strong electronegativity of the N1-O2 locus.

In the AHQ oxidation state, the ^{Bf}AHQ$_{R146}$ model results in a very different distribution of excess electron density from that stabilized in ^{Bf}AHQ$_{xtal}$, with the H-bond from R146 drawing electron density to ^{Bf}O4$_{R146}$ (Fig. 11*A*), rather than ^{Bf}N5 as in ^{Bf}AHQ$_{xtal}$ (Fig. 5). The smaller electron density deficit on O2 in ^{Bf}O2$_{R416}$ may be because O4 is in the *meta*-position relative to O2, whereas N5 is in *para*.

Thus, we have identified H-bonding that can explain an unfavorable electron density deficit at O2 that is particularly acute in the ^{Bf}ASQ (Fig. 5), whereas altered H-bonding in ^{Bf}AHQ$_{R146}$ enables the site to stabilize the same net charge in the AHQ. Together with the native reactivity of flavins, these two features can rationalize the Bf site's suppression of ASQ and 1e reactivity, in favor of the 2e reactivity that characterizes bifurcating sites. This is in striking contrast with the ET site, where 1e reactivity results from stabilization of ASQ we could attribute substantially to H-bonding to O2.

Concluding remarks

We employed computations to learn about reduced states not captured yet in crystal structures, including states such as the postulated high-energy ASQ state of Bf flavin, which is not normally stable enough to permit spectroscopic study. Our calculations assuming the closed conformation reproduce the observed contrasting reactivities of the two flavins. Thus, they succeed in modeling the protein features that stabilize the ASQ state in the ET site but not the Bf site, as well as features that disfavor reduction of the Bf flavin more than the ET flavin. Our calculations show that the extraordinary stability of ^{ET}flavin's ASQ state can be attributed substantially to a single H-bond, from H290 to ^{ET}ASQ's O2. Formation of the AHQ state of ET flavin, including acquisition of a proton at N5, was associated with a change in the preferred orientation of Q266, displacement of a backbone loop, and reorganization of an interaction network spanning domains and subunits. In addition, we raise the possibility that the side chain of R146 reorients upon reduction of the Bf flavin and forms different H-bonds. New H-bond donation to the Bf flavin's O4 is consistent with this flavin's lower $E^{\circ}_{OX/AHQ}$ while the absence of a good H-bond donor to N1 and O2 can explain this flavin's suppressed ASQ that contrasts with that of the ET flavin.

Experimental procedures

General approach

The starting coordinates for the Bf-ETF of *A. fermentans* (*Afe*ETF) were retrieved from the crystal structure (4KPU.pdb (53)). Apart from the crystallographic waters present in the crystal structure, additional water molecules were added with Dowser++ (54) (three water molecules within 5 Å of ^{Bf}FAD and seven water molecules within 5 Å of ^{ET}FAD), resulting in a total 607 water molecules. A total of 11 systems were defined (Table 2), where the oxidation state and selected additional properties of the flavin of interest were varied. The model ^{Bf}AHQ$_{R146}$ will be discussed at the end of this section.

Relaxation via molecular mechanical energy minimization

MM energy minimization was performed with the "pmemd" software from AMBER18 (55) on each of the systems in Table 2. Structures were preprocessed with "tleap" to obtain topology and coordinate files for AMBER (55). The ff19SB force field was defined for protein residues (56), while the

Table 2
Models employed in this study[a]

Name of the model	Description
^{Bf}OX	Bf flavin in oxidized state
^{Bf}ASQ	Bf flavin in anionic semiquinone state
^{Bf}AHQ	Bf flavin in anionic hydroquinone state
^{Bf}AHQ$_{H1}$	^{Bf}AHQ protonated at ^{Bf}N1 instead of ^{Bf}N5
^{Bf}AHQ$_{R146}$	^{Bf}AHQ with alternate rotamer of R146
^{ET}OX$_{\varepsilon}$	ET flavin in oxidized state, ε tautomer of H290
^{ET}ASQ$_{\varepsilon}$	ET flavin in anionic semiquinone state, ε tautomer of H290
^{ET}AHQ$_{\varepsilon}$	ET flavin in anionic hydroquinone state, ε tautomer of H290
^{ET}OX$_{\delta}$	ET flavin in oxidized state, δ tautomer of H290
^{ET}ASQ$_{\delta}$	ET flavin in anionic semiquinone state, δ tautomer of H290
^{ET}AHQ$_{\delta}$	ET flavin in anionic hydroquinone state, δ tautomer of H290

[a] Structural formulae are provided in Figure 2. The term "flavin" is employed to refer specifically to the isoalloxazine head group of FAD, whereas FAD additionally includes adenosine diphosphate (ADP) ribose. A superscripted prefix is employed to specify which of the two flavins/FADs is intended. This notation is also applied to atoms within a flavin (see Figures 2 and 3 for position numbering). OX refers to the oxidized state, ASQ to the anionic semiquinone, ASH to the anionic hydroquinone, NHQ to neutral hydroquinone, and when these occur alone they refer to the flavin, whereas "FAD" is specified when the entire dinucleotide is intended. Residues from the EtfA chain are identified simply by their position number and one-letter code (*e.g.*, R146), whereas residues from the EtfB chain are identified with an apostrophe (*e.g.*, T94′).

GAFF force field was implemented for FAD (57, 58). Parameters for FAD in the canonical oxidation states were calculated with RESP (59) and Antechamber (57, 58, 60). Parameters are listed in SI. Only the $^{Bf}AHQ_{H1}$ system could not be relaxed *via* MM energy minimization, as no parameters were calculated.

The 607 water molecules were defined as TIP3P waters. The total charge of each system was neutralized with addition of Na^+ ions (19 ions in OX systems and 20 ions in ASQ and AHQ systems), which were allowed to adopt energy minimizing locations. The MM energy minimization was performed in two steps, $5{\cdot}10^3$ cycles of steepest descent followed by $5{\cdot}10^3$ cycles using the conjugate gradient method. A restraining force of 100 kcal mol^{-1} $Å^{-2}$ was applied on solute atoms during the energy minimization to prioritize relaxation of solvent. The electrostatic cutoff value was 10 Å, and the effective Born radius was set to 25 Å in lieu of a water box.

The relaxed computational models were assessed using MolProbity, which scores for avoidance of unfavorable Ramachandran angles, van der Waals clashes, and improbable rotamers (61). All the structures of this study displayed MolProbity scores better than that of the parent crystal structure and were in the 100th percentile (Table S13). The RMSD *versus* the crystal structure (4KPU.pdb) was always below 0.85 Å (Table S14).

Hybrid quantum mechanical/molecular mechanical geometry optimization

Geometries were optimized *via* QM/MM energy minimization using B3LYP/cc-pVDZ with D3BJ dispersion correction using the structures obtained from initial MM energy minimization. As no MM energy minimization was performed for the $^{Bf}AHQ_{H1}$ model, relaxed coordinates from the ^{Bf}AHQ model were adopted, the H5 atom was removed, and an H was placed near N1. The QM region consisted of the lumiflavin moiety of the flavin of interest (Fig. 2, 30 atoms in OX and ASQ systems and 31 atoms in AHQ systems). The MM region was defined as the rest of the atoms, where the two following groups of atoms were allowed to move: side chains including an atom within 5 Å of the FAD of interest, and backbone atoms forming H-bonds with the isoalloxazine ring system of interest. The same AMBER force field parameters were employed as for energy minimization, with exception that the cutoff value for nonbonded interactions was defined as 30 Å. Chemshell version 3.7 was employed to interface ORCA 4.2.1 with AMBER18 (55, 62) and to treat the boundary with electrostatic embedding and a hydrogen link scheme (63, 64). QM/MM geometry optimizations were performed using the "DL-FIND" module (65).

H-bonds are understood to combine some covalent character with a predominantly electrostatic (Coulomb) attraction. The covalent component includes steric constraints to produce orientational preferences for shorter H-bonds (66, 67), while the electrostatic component extends over longer distances (47, 68, 69). Although distance between donor and acceptor is not an ideal criterion for determining whether or not an H-bond is present (70), it is well understood and readily measured. A comparison of heavy atom to heavy atom distances deemed to encompass the majority of H-bonds in proteins yields a maximal separation of 3.2 Å for the types of H-bonds we studied (71, 72), which mostly involve an NH group as the H-bond donor and an O as the recipient. OH donors are recognized to produce slightly shorter H-bonds while N atom acceptors produce slightly longer ones (47, 71, 72); however, considering that our uncertainties are on the order of these 0.1 Å differences, we retained a common upper limit of 3.2 Å for the sake of simplicity. In addition, the distance between the acceptor heavy atom and the H atom mediating the interaction is 2.1 Å or shorter in 80 to 90% of H-bonds in a survey of high-resolution crystal structures (47). To provide an inclusive picture, instances satisfying either of these conditions were deemed to represent H-bonds. Interactions over longer distances and a wide range of geometries have been noted in networks of multiple H-bonds (73), especially in connection with aliphatic hydroxyl groups (47). We interpreted these as weaker interactions that are expected to lack orientational preference due to negligible covalent character (47). Therefore, they are described as "H-mediated interactions" (72). Throughout, "donation" or "acceptance" of an H-bond is discussed in terms of donation/acceptance of the H.

Free energy changes associated with reduction and proton acquisition

Free energy changes between flavin oxidation states were calculated to assess energies associated with reduction and proton acquisition. These values do not correspond to E°s because the two states being compared have different numbers of electrons (and protons). However, the energies associated with a given change can be compared for the two flavin sites, to learn which site best stabilizes reduction or proton acquisition, and to ask how the effect is produced by the protein environment. Gibbs free energy values were calculated using QM/MM and the same level of theory as for the geometry optimizations.

As reference, the corresponding free energy changes were calculated for isolated lumiflavin. Density functional theory (DFT) geometry optimizations were performed for lumiflavin in the OX, ASQ, and AHQ states in gas phase with B3LYP/cc-pVDZ and D3BJ dispersion correction. Gibb's free energy values were calculated using DFT using the same level of theory as for the geometry optimizations.

Calculation of Natural Bond Order electron densities in presence and absence of protein environment

Calculations of NBOs of flavin models were performed in the presence and absence of the protein environment using the optimized QM/MM geometries. In the latter case, point charges in the protein were omitted but the optimized QM/MM flavin geometry was retained. Therefore, calculations in the absence of the protein environment were called "frozen gas-phase" NBO. The same level of theory was implemented as for QM/MM and energy calculation.

Relaxed energy scans along N5 and O2 H-bonds

The QM region was enlarged for the following QM/MM calculations to include the side chain atoms of the amino acid participating in the H-bond of interest (18 more atoms for R146, 5 atoms for S270, and 11 atoms for H290). Geometries were reoptimized applying the enlarged QM regions with B3LYP/cc-pVDZ and dispersion correction as in previous sections. Subsequently, two constraints were implemented, similarly to Tsujimura and Ishikita (45): the distance between the participating proton and the H-bond acceptor and the distance between the two heavy atoms of the H-bond. These distances were constrained with a harmonic constant of 6 Hartree/Bohr^2. The reference distance between the H-bond acceptor and the proton was varied in 0.1 Å steps, whereas the reference distance between heavy atoms was set to the previously optimized QM/MM values. In performing relaxed energy scans, the relaxed geometry with the most similar constraint value was used as input for the next constrained geometry optimization.

For each proton position, the Gibbs free energy was calculated using QM/MM and the same level of theory as for the geometry optimizations. These values are plotted *versus* proton–H-bond acceptor distance in the figures. Difficulties were encountered in the Gibbs free energy calculation for the energy-relaxed scans of the N5 H-bond of the $^{ET}ASQ_{\varepsilon}$ and $^{ET}ASQ_{\delta}$ models. For these energy scans, only electronic energies are reported here. We attribute the difficulties to the large distance between the flavin and the S270 side chain.

Local energy minima were validated *via* frequency analysis with DFT using B3LYP/cc-pDVZ and D3BJ dispersion correction. Coordinates of the lumiflavin moiety of the studied flavin and those of all residues in the first coordination sphere were included (266 atoms in ^{Bf}OX and ^{Bf}ASQ; 270 atoms in ^{Bf}AHQ and $^{Bf}AHQ_{H1}$; 257 atoms in $^{ET}OX_{\varepsilon}$; 254 atoms in $^{ET}OX_{\delta}$; 248 atoms in $^{ET}ASQ_{\varepsilon}$; 251 atoms in $^{ET}ASQ_{\delta}$; 252 atoms in $^{ET}AHQ_{\varepsilon}$; and 249 in $^{ET}AHQ_{\delta}$ models).

Additional models

For ^{Bf}flavin, additional models were considered. Working with the coordinates of the OX crystal structure 4KPU.pdb (53), we screened all the rotamers of R146 in Chimera's library (74, 75), reorienting the nearby side chain of C128 when warranted. Most rotamers were excluded on the basis of steric clashes. The two that minimized clashes and formed an H-bond with the flavin were refined by MM energy minimization followed by hybrid QM/MM geometry optimization with the AHQ state of the ^{Bf}flavin, implementing the standard protocol (above). One of the resulting structures had an energy only 1 kcal/mol higher than that of the ^{Bf}AHQ obtained from the crystal structure and was considered further as $^{Bf}AHQ_{R146}$ (Table 2).

We also screened alternative rotamers of the other amino acid side chain capable of H-bonding with the ^{Bf}flavin: T94'. After energy minimization, none H-bonded with the flavin. Indeed, the corresponding residue is Val in a lactate dehydrogenase-associated Bf-ETF (16), demonstrating that H-bonding from the side chain is not mandatory.

Data availability

Data are provided either within the article or as part of the supporting information.

Supporting information—This article is accompanied by supporting information (14–16, 19, 53).

Author contributions—M. G.-V., A.-F. M., M.-A. M. conceptualization; R. K. K., M.-A. M. methodology; M. G.-V., A.-F. M. validation; M. G.-V. investigation; A.-F. M., M.-A. M. resources; M. G.-V., A.-F. M. writing – original draft; M. G.-V., A.-F. M., M.-A. M. writing – review & editing; M. G.-V., A.-F. M. visualization; R. K. K., A.-F. M., M.-A. M. supervision; M.-A. M. project administration; A.-F. M., M.-A. M. funding acquisition.

Funding and additional information—A.-F. M. is pleased to acknowledge partial support from D.O.E. DESC0021283 and KY-EPSCoR PON2 635 2000003148 for investigations of mechanisms for coupling conformational change to flavin-redox events and from N.S.F. CHE 2108134 for investigations of H-bonding as a mechanism tuning flavin reduction midpoint potentials. A.-F. M. acknowledges WDW for vital assistance, and RNM for perseverance. We thank the Einstein Foundation of Berlin for funding to R. K. K., a visiting fellowship to A.-F. M., and ongoing support to M. G.-V. *via* the Einstein Center for Catalysis. M.-A. M.'s research was funded by the Deutsche Forschungsgemeinschaft (DFG, German Research Foundation) under SFB1078, project C2. R. K. K. thanks DST-SERB for a start-up grant (SRG/2022/000858).

Conflict of interest—The authors declare that they have no conflicts of interest with the contents of this article.

Abbreviations—The abbreviations used are: *Afe*ETF, Bf-ETF of *Acidaminococcus fermentans*; AHQ, anionic hydroquinone; ASQ, anionic semiquinone; Bf-ETF, bifurcating electron transferring flavoprotein; ET, electron transfer; ETF, electron transferring flavoprotein; FAD, flavin adenine dinucleotide; HQ, hydroquinone; MM, molecular mechanical; OX, oxidized state; QM, quantum mechanical; SQ, semiquinone.

References

1. Beinert, H. (1956) Spectral characteristics of flavins at the semiquinoid oxidation level. *J. Am. Chem. Soc.* **78**, 5323–5328
2. Thorpe, C. (1991) Electron-transferring flavoproteins. In: Müller, F., ed. *Chemistry and Biochemistry of Flavoenzymes*, CRC press, Boca Raton FL: 471–486
3. Watmough, N. J., Kiss, J., and Frerman, F. E. (1992) Structural and redox relationships between Paracoccus denitrificans, porcine and human electron-transferring flavoproteins. *Eur. J. Biochem.* **205**, 1089–1097
4. Toogood, H. S., van Thiel, A., Scrutton, N. S., and Leys, D. (2005) Stabilization of non-productive conformations underpins rapid electron transfer to electron transferring flavoprotein. *J. Biol. Chem.* **280**, 30361–30366
5. Whitfield, C. D., and Mayhew, S. G. (1974) Purification and properties of electron-transferring flavoprotein from *Peptostreptococcus elsdenii*. *J. Biol. Chem.* **249**, 2801–2810
6. Mohamed-Raseek, N., Duan, H. D., Mroginski, M. A., and Miller, A. F. (2019) Spectroscopic, thermodynamic and computational evidence of the locations of the FADs in the nitrogen fixation-associated electron transfer flavoprotein. *Chem. Sci.* **10**, 7762–7772
7. DuPlessis, E. R., Rohlfs, R. J., Hille, R., and Thorpe, C. (1994) Electron-transferring flavoproteins from pig and the methylotrophic bacterium

W3A1 contains AMP as well as FAD. *Biochem. Mol. Biol. Int.* **32**, 195–199
8. Sato, K., Nishina, Y., and Shiga, K. (1993) Electron-transferring flavoprotein has an AMP-binding site in addition to the FAD-binding site. *J. Biochem.* **114**, 215–222
9. Nitschke, W., and Russell, M. J. (2012) Redox bifurcations: mechanisms and importance to life now, and at its origin. *Bioessays* **34**, 106–109
10. Buckel, W., and Thauer, R. K. (2018) Flavin-based electron bifurcation, a new mechanism of biological energy coupling. *Chem. Rev.* **118**
11. Peters, J. W., Miller, A. F., Jones, A. K., King, P. W., and Adams, M. W. (2016) Electron bifurcation. *Curr. Opin. Chem. Biol.* **31**, 146–152
12. Buckel, W., and Thauer, R. K. (2013) Energy conservation *via* electron bifurcating ferredoxin reduction and proton/Na+ translocating ferredoxin oxidation. *Biochim. Biophys. Acta* **1827**, 94–113
13. Herrmann, G., Jayamani, E., Mai, G., and Buckel, W. (2008) Energy conservation *via* electron-transferring flavoprotein in anaerobic bacteria. *J. Bacteriol.* **190**, 784–791
14. Demmer, J. K., Bertsch, J., Oppinger, C., Wohlers, H., Kayastha, K., Demmer, U., *et al.* (2018) Molecular basis of the flavin-based electron-bifurcating caffeyl-CoA reductase reaction. *FEBS Lett.* **592**, 332–342
15. Demmer, J. K., Chowdhury, N. P., Selmer, T., Ermler, U., and Buckel, W. (2017) The semiquinone swing in the bifurcating electron transferring flavoprotein/butyryl-coA dehydrogenase complex from *Clostridium difficile*. *Nat. Commun.* **8**, 1577
16. Kayastha, K., Katsyv, A., Himmrich, C., Welsch, S., Schuller, J. M., Ermler, U., *et al.* (2022) Structure-based electron-confurcation mechanism of the Ldh-EtfAB complex. *eLife* **11**, e77095
17. Duan, H. D., Mohamed-Raseek, N., and Miller, A. F. (2020) Spectroscopic evidence for direct flavin-flavin contact in a bifurcating electron transfer flavoprotein. *J. Biol. Chem.* **295**, 12618–12634
18. Leys, D., Basran, J., Talfournier, F., Sutcliffe, M. J., and Scrutton, N. S. (2003) Extensive conformational sampling in a ternary electron transfer complex. *Nat. Struct. Biol.* **10**, 219–225
19. Feng, X., Schut, G. J., Lipscomb, G., Li, H. Y., and Adams, M. W. W. (2021) Cryoelectron microscopy structure and mechanism of the membrane-associated electron-bifurcating flavoprotein Fix/EtfABCX. *Proc. Natl. Acad. Sci. U. S. A.* **118**, e2016978118
20. Duan, H. D., Lubner, C. E., Tokmina-Lukaszewska, M., Gauss, G. H., Bothner, B., King, P. W., *et al.* (2018) Distinct flavin properties underlie flavin-based electron bifurcation within a novel electron-transferring flavoprotein FixAB from *Rhodopseudomonas palustris*. *J. Biol. Chem.* **293**, 4688–4701
21. Schut, G. J., Mohamed-Raseek, N. R., Tokmina-Lukaszewska, M., Mulder, D. E., Nguyen, D. M. N., Lipscomb, G. L., *et al.* (2019) The catalytic mechanism of electron bifurcating electron transfer flavoproteins (ETFs) involves an intermediary complex with NAD+. *J. Biol. Chem.* **294**, 3271–3283
22. Massey, V., and Hemmerich, P. (1980) Active site probes of flavoproteins. *Biochem. Soc. Trans.* **8**, 246–257
23. Fagan, R. L., and Palfey, B. A. (2010) Flavin-dependent enzymes. In: Begley, T., ed. *Comprehensive Natural Products Chemistry II*, Elsevier, Oxford, UK: 37–114
24. Mayhew, S. G. (1999) The effects of pH and semiquinone formation on the oxidation-reduction potentials of flavin mononucleotide: a reappraisal. *Eur. J. Biochem.* **265**, 698–702
25. Land, E. J., and Swallow, A.,J. (1966) One-electron reactions in biochemical systems as studied by pulse radiolysis. II. Riboflavine. *Biochem* **5**, 2117–2125
26. Roberts, D. L., Salazar, D., Fulmer, J. P., Frerman, F. E., and Kim, J. J. (1999) Crystal structure of paracoccus denitrificans electron transfer flavoprotein: structural and electrostatic analysis of a conserved flavin binding domain. *Biochemistry* **38**, 1977–1989
27. Iijima, M., Ohnuki, J., Sato, T., Sugishima, M., and Takano, M. (2019) Coupling of redox and structural states in cytochrome P450 reductase studied by molecular dynamics simulation. *Sci. Rep.* **9**, 9341
28. Walsh, J. D., and Miller, A.-F. (2003) Flavin reduction potential tuning by substitution and bending. *J. Mol. Struct. (Theochem)* **623**, 185–195
29. Hasford, J. J., Kemnitzer, W., and Rizzo, C. J. (1997) Conformational effects on flavin redox chemistry. *J. Org. Chem.* **62**, 5244–5245
30. Hazekawa, I., Nishina, Y., Sato, K., Shichiri, M., Miura, R., and Shiga, K. (1997) A Raman study on the C(4)=O stretching mode of flavins in flavoenzymes: hydrogen bonding at the C(4)=O moiety. *J. Biochem.* **121**, 1147–1154
31. Wille, G., Ritter, M., Friedemann, R., Mantele, W., and Hubner, G. (2003) Redox-triggered FTIR difference spectra of FAD in aqueous solution and bound to flavoproteins. *Biochemistry* **42**, 14814–14821
32. Rüterjans, H., Fleischmann, G., Löhr, M., Knauf, F., Blümel, M., Lederer, F., *et al.* (1996) NMR studies of flavoproteins. *Biochem. Soc. Trans.* **24**, 116–121
33. Cui, D., Koder, R. L., Jr., Dutton, P. L., and Miller, A.-F. (2011) ^{15}N solid-state NMR as a probe of flavin H-bonding. *J. Phys. Chem. -B.* **115**, 7788–7798
34. Mohamed-Raseek, N., and Miller, A. F. (2022) Contrasting roles for two conserved arginines: Stabilizing flavin semiquinone or quaternary structure, in bifurcating electron transfer flavoproteins. *J. Biol. Chem.* **298**, 101733
35. Dwyer, T. M., Zhang, L., Muller, M., Marrugo, F., and Frerman, F. E. (1999) The functions of the flavin contact residues αArg249 and βTyr16, in human electron transfer flavoprotein. *Biochim. Biophys. Acta* **1433**, 139–152
36. Talfournier, F., Munro, A. W., Basran, J., Sutcliffe, M. J., Daff, S., Chapman, S. K., *et al.* (2001) Alpha Arg-237 in *Methylophilus methylotrophus* (sp. W3A1) electron-transferring flavoprotein affords approximately 200-millivolt stabilization of the FAD anionic semiquinone and a kinetic block on full reduction to the dihydroquinone. *J. Biol. Chem.* **276**, 20190–20196
37. Yang, K. Y., and Swenson, R. P. (2007) Modulation of the redox properties of the flavin cofactor through hydrogen-bonding interactions with the N(5) atom: role of alpha Ser254 in the electron-transfer flavoprotein from the methylotrophic bacterium W3A1. *Biochem* **46**, 2289–2297
38. Garcia Costas, A. M., Poudel, S., Miller, A.-F., J, S. G., Ledbetter, R. N., Fixen, K., *et al.* (2017) Defining electron bifurcation in the electron transferring flavoprotein family. *J. Bacteriol.* **199**, e00440-17
39. Sucharitakul, J., Buttranon, S., Wongnate, T., Chowdhury, N. P., Prongjit, M., Buckel, W., *et al.* (2020) Modulations of the reduction potentials of flavin-based electron bifurcation complexes and semiquinone stabilities are key to control directional electron flow. *FEBS J.* https://doi.org/10.1111/febs.15343
40. Ludwig, M. L., Pattridge, K. A., Metzger, A. L., Dixon, M. M., Eren, M., Feng, Y., *et al.* (1997) Control of oxidation-reduction potentials in flavodoxin from *Clostridium beijerinckii*: the role of conformational changes. *Biochemistry* **36**, 1259–1280
41. Foster, J. P., and Weinhold, F. (1980) Natural bond orbitals. *J. Am. Chem. Soc.* **102**, 7211
42. Zhang, Y.-L., Wang, F.-L., and Ren, A.-M. (2022) Reliability of computed molecular structures. *J. Comp. Chem.* **43**, 465–476
43. Unno, M., Masuda, S., Ono, T., and Yamauchi, S. (2006) Orientation of a key glutamine residue in the BLUF domain from AppA revealed by mutagenesis, spectroscopy, and quantum chemical calculations. *J. Am. Chem. Soc.* **128**, 5638–5639
44. Domratcheva, T., Hartmann, E., Schlichting, I., and Kottke, T. (2016) Evidence for tautomerisation of glutamine in BLUF blue light receptors by vibrational spectroscopy and computational chemistry. *Sci. Rep.* **6**, 22669
45. Tsujimura, M., and Ishikita, H. (2021) Identification of intermediate conformations in the photocycle of the light-driven sodium-pumping rhodopsin KR2. *J. Biol. Chem.* **296**, 100459
46. Wendler, K., Thar, J., Zahn, S., and Kirchner, B. (2010) Estimating the hydrogen bond energy. *J. Phys. Chem.* **114**, 9529–9536
47. O'Meara, M. J., Leaver-Fay, A., Tyka, M. D., Stein, A., Houlihan, K., DiMaio, F., *et al.* (2015) Combined covalent-electrostatic model of hydrogne bonding improves structure prediction with rosetta. *J. Chem. Theor. Comput.* **11**, 609–622
48. Dwyer, T. M., Mortl, S., Kemter, K., Bacher, A., Fauq, A., and Frerman, F. E. (1999) The intraflavin hydrogen bond in human electron transfer

flavoprotein modulates redox potentials and may participate in electron transfer. *Biochem* **38**, 9735–9745
49. Hall, L. H., Bowers, M. L., and Durfor, C. N. (1987) Further consideration of flavin coenzyme biochemistry afforded by geometry-optimized molecular orbital calculations. *Biochemistry* **26**, 7401–7409
50. Virgil, W., Jr., Tran, J., Niks, D., Schut, G. J., Ge, X., Adams, M. W. W., *et al.* (2022) The reductive half-reaction of two bifurcating electron-transferring flavoproteins: evidence for changes in flavin reduction potentials mediated by specific conformational changes. *J. Biol. Chem.* **298**, 101927
51. Yikilmaz, E., Rodgers, D. W., and Miller, A.-F. (2006) The crucial importance of chemistry in the structure-function link: manipulating hydrogen bonding in iron-containing superoxide dismutase. *Biochemistry* **45**, 1151–1161
52. Walsh, J. D., and Miller, A.-F. (2003) NMR shieldings and electron correlation reveal remarkable behaviour on the part of the flavin N_5 reactive center. *J. Phys. Chem. B* **107**, 854–863
53. Chowdhury, N. P., Mowafy, A. M., Demmer, J. K., Upadhyay, V., Koelzer, S., Jayamani, E., *et al.* (2014) Studies on the mechanism of electron bifurcation catalyzed by electron transferring flavoprotein (Etf) and butyryl-CoA dehydrogenase (Bcd) of *Acidaminococcus fermentans*. *J. Biol. Chem.* **289**, 5145–5157
54. Morozenko, A., and Stuchebrukhov, A. A. (2016) Dowser++, a new method of hydrating protein structures. *Proteins, Struct. Funct. Bioinform.* **84**, 1347–1357
55. Case, D. A., Ben-Shalom, I. Y., Brozell, S. R., Cerutti, D. S., Cheatham, I., T, E., *et al.* (2018) *AMBER 2018*, University of California, San Francisco., San Francisco
56. Tian, C., Kasavajhala, K., A, K. A., Belfon, K. A. A., Raguette, L., Huang, H., *et al.* (2020) ff19SB: Amino-Acid-Specific protein backbone parameters trained against quantum mechanics energy surfaces in solution. *J. Chem. Theor. Comput.* **16**, 528–552
57. Wang, J., Wolf, R. M., Caldwell, J. W., Kollman, P. A., and Case, D. A. (2004) Development and testing of a general AMBER force field. *J. Comp. Chem.* **25**, 1157–1174
58. Wang, J., Wang, W., A, K. P., and Case, D. A. (2006) Automatic atom type and bond type perception in molecular mechanical calculations. *J. Mol. Graph. Model.* **25**, 247260
59. Bayly, C. I., Cieplak, P., Cornell, W., and Kollman, P. A. (1993) A well-behaved electrostatic potential based method using charge restraints for deriving atomic charges: the RESP model. *J. Phys. Chem.* **97**, 10269–10280
60. Wei, B. Q., Weaver, L. H., Ferrari, A. M., Matthews, B. W., and Soichet, B. K. (2004) Testing a flexible-receptor docking algorithm in a model binding site. *J. Mol. Bio.* **337**, 1161–1182
61. Williams, C. J., Headd, J. J., Moriarty, N. W., Prisant, M. G., Videau, L. L., Deis, L. N., *et al.* (2017) MolProbity: more and better reference data for improved all-atom structure validation. *Prot. Sci.* **27**, 293–315
62. Neese, F., Wennmohs, F., Becker, U., and Riplinger, C. (2020) The ORCA quantum chemistry program package. *J. Chem. Phys.* **152**, 224108
63. Lu, Y., Farrow, M. R., Fayon, P., Logsdail, A. J., Sokol, A. A., Catlow, C. R. A., *et al.* (2019) Open-source, python-based redevelopment of the ChemShell multiscale QM/MM environment. *J. Chem. Theor. Comput.* **15**, 1317
64. Sherwood, P., de Vries, A. H., Guest, M. F., Schreckenbach, G., Catlow, C. R. A., French, S. A., *et al.* (2003) Quasi: a general purpose implementation of the QM/MM approach and its application to problems in catalysis. *J. Mol. Str.* **632**, 1–28
65. Kästner, J., Carr, J. M., Keal, T. W., Thiel, W., Wander, A., and Sherwood, P. (2009) DL-FIND: an open-source geometry optimizer for atomistic simulations. *J. Phys. Chem. A.* **113**, 11856–11865
66. Kulik, H. J., Luehr, N., Ufimtsev, I. S., and Martinez, T. J. (2012) *Ab initio* quantum chemistry for protein structures. *J. Phys. Chem. B* **116**, 12501–12509
67. Morozov, A. V., Kortemme, T., Tsemekhman, K., and Baker, D. (2004) Close agreement between the orientation dependence of hydrogen bonds observed in protein structures and quantum mechanical calculations. *Proc. Natl. Acad. Sci. U. S. A.* **101**, 6946–6951
68. L, P., W, J., C, and T, V. V. (2013) Systematic parametrization of polarizable force fields from quantum chemistry data. *J. Chem. Theor. Comput.* **9**, 452–460
69. Ponder, J., and Case, D. (2003) Force fields for protein simulations. *Adv. Protein Chem.* **66**, 27–65
70. Arunan, E., Desiraju, G. R., Klein, R. A., Sadlej, J., Scheiner, S., Alkorta, I., *et al.* (2011) Definition of the hydrogen bond (IUPAC Recommendations 2011). *Pure Appl. Chem.* **83**, 1637–1641
71. Herschlag, D., and Pinney, M. M. (2018) Hydrogen bonds: simple after all? *Biochem* **57**, 3338–3352
72. Merski, M., Skrzeczkowski, J., Roth, J. K., and Górna, M. W. (2020) A geometric definition of short to medium ranage hydrogen-mediated interactions in proteins. *Molecules* **25**, 5326
73. Stranges, P. B., and Kuhlman, B. (2013) A comparison of successful and failed protein interface designs highlights the challenges of designing buried hydrogen bonds. *Prot. Sci.* **22**, 74–82
74. Meng, E. C., Pettersen, E. F., Couch, G. S., Huang, C. C., and Ferrin, T. E. (2006) Tools for integrated sequence-structure analysis with UCSF Chimera. *BMC Bioinform.* **7**, 339
75. Pettersen, E. F., Goddard, T. D., Huang, C. C., Couch, G. S., Greenblatt, D. M., Meng, E. C., *et al.* (2004) UCSF Chimera - a visualization system for exploratory research and analysis. *J. Comput. Chem.* **25**, 1605–1612